Cancer Research

CircNT5E Acts as a Sponge of miR-422a to Promote Glioblastoma Tumorigenesis

Renjie Wang[1,2], Sai Zhang[1,2], Xuyi Chen[1,2], Nan Li[1,2], Jianwei Li[1,2], Ruichao Jia[1,2], Yuanqing Pan[3], and Haiqian Liang[1,2,4]

Abstract

Circular RNA and long noncoding RNA function as efficient miRNA sponges that regulate gene expression in eukaryotes. However, the sponges of functional miRNAs in glioblastoma remain largely unknown. Here, we identify a subset of circRNAs and lncRNAs that are specifically increased in miR-422a–downregulated glioblastoma tissues. We characterized a novel circRNA derived from NT5E, named circNT5E, that is regulated by ADARB2 binding to sites flanking circRNA-forming introns. We hypothesized that circNT5E may serve as a sponge against miR-422a in glioblastoma tumorigenesis. circNT5E controlled multiple pathologic processes, including cell proliferation, migration, and invasion. circNT5E directly bound miR-422a and inhibited miR-422a activity. Furthermore, circNT5E was observed to sponge other miRNAs, exhibiting tumor suppressor–like features in glioblastoma. Taken together, these findings highlight a novel oncogenic function of circRNA in glioblastoma tumorigenesis.

Significance: Microarray profiling of circRNA/lncRNA/mRNA in glioblastoma identifies circNT5E as an oncogenic circular RNA and a sponge of miR-422a. *Cancer Res; 78(17); 4812–25. ©2018 AACR.*

Introduction

Glioblastoma (GBM) is well-known as the most common primary aggressive malignant brain tumor of the central nervous system and one of the most lethal forms of cancer in humans (1, 2). Following maximum feasible surgical resection, patients treated with radiotherapy and temozolomide chemotherapy show a median overall survival of approximately 15 months (3, 4). Patients with GBM may benefit from additional treatment, such as personalized therapies against molecular targets, but many potential treatments have been unsuccessful in clinical trials or have strong side effects (5, 6). Therefore, novel treatment approaches, specifically those targeting the complex gene regulation network, are urgently needed for GBM.

Noncoding RNAs (ncRNA), which comprise various RNAs, including miRNAs, long noncoding RNAs (lncRNA), and circular RNAs (circRNA), play crucial roles in cell development and disease (7–11). Among them, circRNAs represent a widespread class of ncRNAs that are generated by back-splicing and are characterized as covalently closed loop structures with neither 5′ to 3′ polarity nor a polyadenylated tail (12, 13). With the advent of next-generation sequencing and bioinformatics, circRNAs have been detected in various eukaryotes and have been shown to participate in the pathology of disease (14–17). Three important functions of circRNAs have been identified: (i) circRNAs function as "miRNA sponges" (18–20); (ii) circRNAs bind to RNA-binding proteins (21); and (iii) circRNAs can undergo translation (22–24). The first function of circRNA, termed the competitive endogenous RNA (ceRNA) hypothesis, has been observed empirically, but the results are controversial (25–27). Currently, two important circRNAs, *cIRS-7*/*CDR1as* and *Sry*, which harbor many conventional miRNA-binding sites, have been identified as miRNA inhibitors (13, 20). In addition, the functions of circRNAs (including circSMARCA5, circMTO1, circCCDC66, circTTBK2, and circZNF292), particularly their ability to bind miRNAs in hepatocellular carcinoma, colorectal cancer, and glioma pathologies, have been revealed (28–32).

miRNAs belonging to the other types of ncRNAs, which are highly conserved across species, regulate gene expression by binding to the 3′-untranslated region of the target mRNAs and play central roles in the ceRNA hypothesis (33, 34). In recent years, our group has focused on the role of brain-enriched miRNAs, such as miR-422a, in GBM (35). Other groups have shown that miR-422a plays crucial roles in head and neck squamous cell carcinoma, squamous cell lung cancer, and glioma pathology (36–38). However, very little is known about miRNAs related to the upstream regulators of GBM; these miRNAs may block tumorigenesis and function as molecular targets in GBM treatment.

In this study, we detected hundreds of circRNAs and lncRNAs that were upregulated in miR-422a–downregulated GBM tissues. We screened 38 circRNAs/lncRNAs with a high potential to sponge miR-422a by using a bioinformatics method. Then, biotin–miRNA pull-down assays revealed that has_circ_0077232 had the highest fold change for bio-miR-422a capture. This finding implies that hsa_circ_0077232 (circNT5E) may be a novel oncogene in GBM tumorigenesis because it affects

[1]Institute of Traumatic Brain Injury and Neurology, Pingjin Hospital, Logistics University of Chinese People's Armed Police Forces, Tianjin, China. [2]Department of Neurosurgery, Pingjin Hospital, Logistics University of Chinese People's Armed Police Forces, Tianjin, China. [3]Department of Basic Medicine, Tianjin Medical College, Tianjin, China. [4]Chinese Glioma Cooperative Group (CGCG), China.

Note: Supplementary data for this article are available at Cancer Research Online (http://cancerres.aacrjournals.org/).

Corresponding Author: Haiqian Liang, Pingjin Hospital, Logistics University of Armed Police Forces, No. 220, Chenglin Road, Tianjin 300162, China. Phone: 8602260577125; Fax: 8602260577125; E-mail: lianghaiqian711@163.com

doi: 10.1158/0008-5472.CAN-18-0532

miR-422a. Furthermore, we found that circNT5E affects the proliferation, apoptosis, migration, and invasion abilities of GBM cells *in vitro* and *in vivo*. In addition, we revealed that adenosine deaminase, RNA-specific, B2 (ADARB2), and long intronic complementary repeat elements were involved in the formation and regulation of circNT5E. qRT-PCR assays revealed that circNT5E inhibited multiple GBM-suppressor miRNAs. Therefore, circNT5E may function as a binding platform for GBM-suppressor miRNAs and thus may be a novel therapeutic target for treating GBM.

Materials and Methods

Clinical samples

Tumor tissue samples and adjacent normal tissues (ANT) from 39 patients with glioma (including 18 with GBM) were collected from the surgical specimen archives of Pingjin Hospital, Tianjin, China, between January 2014 and May 2017 with written-informed consent from the patients. All the procedures were approved by the Institutional Review Board of Pingjin Hospital, Logistics University of Chinese People's Armed Police Forces, and conducted in accordance with the Declaration of Helsinki. All tissues were placed immediately in liquid nitrogen after removal from the glioma patients and stored at –80°C until use. Detailed patient information is shown in Supplementary Table S1.

Microarray

Total RNA was extracted and purified using the mirVana miRNA Isolation Kit (Cat. #AM1561; Ambion) according to the manufacturer's instructions and then evaluated for its RIN number to determine RNA integration with an Agilent Bioanalyzer 2100 (Agilent Technologies). Total RNA was amplified and labeled with a Low Input Quick Amp WT Labeling kit (Cat. # 5190-2943; Agilent Technologies). Labeled cRNA was purified with an RNeasy Mini Kit (Cat. #74106;Qiagen).

Each slide was hybridized with 1.65 μg Cy3-labeled cRNA using a Gene Expression Hybridization kit (Cat. #5188-5242; Agilent Technologies) in a hybridization oven (Cat. #G2545A; Agilent Technologies). After 17 hours of hybridization, the slides were washed in staining dishes (Cat. # 121; Thermo Scientific) with a Gene Expression Wash Buffer kit (Cat. #5188-5327; Agilent Technologies).

The slides were scanned with an Agilent Microarray Scanner (Cat. #G2565CA; Agilent Technologies) with the following default settings: dye channel, green; scan resolution, 3 μm; PMT, 100%; 20 bit. The data were extracted with Feature Extraction software 10.7 (Agilent Technologies). The raw data were normalized using the Quantile algorithm of the limma package in R. A microarray analysis was performed by Shanghai Biotechnology Cooperation.

Cell culture and treatment

GBM cells (U87 and U251) were purchased from the Shanghai Institute of Biochemistry and Cell Biology, Chinese Academy of Sciences (Shanghai, China). All cell lines were determined to be mycoplasma-free. U87 and U251 cells were maintained in DMEM. All culture media contained 10% FBS (Gibco), 100 U/mL penicillin, and 100 U/mL streptomycin (Invitrogen). All cells were grown at 37°C and 5% CO_2 saturation. The culture medium was replaced every 2 to 3 days. Cells were digested with 0.25% trypsin when they reached 80% to 90% confluence, and 5×10^5 cells were then added to culture bottles (25 cm^2, Corning, Inc.).

Vector construction and stable transfection

A human circNT5E expression vector, si-circNT5E expression vector, lentivirus-si-circNT5E, and lentivirus-circNT5E were purchased from GenePharma. Lentiviruses were ultracentrifuged, concentrated, and validated. Transfected cells were selected with puromycin (Solarbio) for 1 week. The surviving cells were used as stable mass transfectants. Human ADARB2 from HEK293T cells was amplified by PCR. The PCR products were inserted into the pcDNA3.1/EGFP vector between the BglII and BamHI sites.

RNA preparation, treatment with RNase R, and PCR

Total RNA was extracted from the treated cells and tissues by using Trizol reagent (TransGen Biotech) according to the manufacturer's instructions. For RNase R treatment, 2 mg total RNA was incubated for 15 minutes at 37°C with or without 3 U/mg RNase R (Epicentre Technologies). qRT-PCR was performed by using SYBR Green (TransGen Biotech) according to the manufacturer's instructions. The results were measured on an ABI 7500 real-time PCR instrument (Applied Biosystems). The relative mRNA expression levels were analyzed using the $2^{-\triangle\triangle C_t}$ method. The primers and RNA sequences are shown in Supplementary Table S2.

FISH

Briefly, FITC-labeled circNT5E and Cy3-labeled miR-422a probes were designed and synthesized by Songan Biotech; the probe sequences are available upon request. The probe signals were detected with a fluorescent in situ hybridization kit (RiboBio) according to the manufacturer's instructions. To determine the circNT5E status in normal and World Health Organization (WHO) I, WHO II, WHO III, and WHO IV GMB tissues, 4-μm-thick sections were cut from paraffin-embedded blocks, and the sections were processed, hybridized, and analyzed. The labeled probe flanking circNT5E was applied to the samples. The cells were treated with 4′-6-diamidino-2-phenylindole (DAPI; Life Technologies) as a control. The results were observed under a fluorescence microscope (Eclipse E600; Nikon Corporation). Confocal images were acquired on a Leica SP5 confocal microscope (Leica Microsystems).

Pull-down assay with biotinylated miRNA and Alusq

The capture of miR-422a–bound ceRNAs in a pull-down assay with biotinylated miR-422a was performed as described previously (25, 39). Briefly, GBM cells were transfected with biotinylated miRNA mimics or controls (50 nmol/L) and harvested at 48 hours after transfection. The biotin-coupled RNA complex was pulled down by incubating the cell lysates with streptavidin-coated magnetic beads (No. 88817, Pierce Biotechnology). The bound RNA was purified using an RNeasy Mini Kit (QIAGEN) for analysis. The abundance of ceRNA in the bound fractions was evaluated by qRT-PCR analysis. To capture the Alusq-bound proteins in a pull-down assay with biotin-Alusq, Alusq was transcribed *in vitro* using a T7 high-efficiency transcription kit (Cat. #JT1-1-01, TransGen Biotech); then, a single biotin was attached by using a Pierce RNA 3′End Desthiobiotinylation Kit (No. 20163, Pierce Biotechnology). The RNA-protein pull-down assay was then performed (Pierce Magnetic RNA-Protein Pull-Down Kit, No. 20164, Pierce Biotechnology). The primer sequences are listed in Supplementary Table S2.

Target DNA deletion by CRISPR/Cas9 technology

U87 cells (1×10^5 cells/well) were seeded in 12-well plates and incubated for 24 hours at 37°C. The cells were then transfected with pYSY-CMV-Cas9-U6-sgRNA-EFla-eGFP/puromycin/mcherry plasmids using Lipofectamine 3000 (Invitrogen) according to the manufacturer's protocol. Genomic DNA was extracted using QuickExtract DNA Extraction Solution (Yao Shun Yun Biotech). PCR was performed to amplify specific genes. The primer sequences are presented in Supplementary Table S2.

Oligonucleotide transfection

miRNA mimics, inhibitors, and primers were synthesized by Gene-Pharma. The sequences used are listed in Supplementary Table S2. Transfection was carried out using Lipofectamine 3000 (Invitrogen; Thermo Fisher Scientific, Inc.) according to the manufacturer's instructions. Original or stable U87 and U251 cells (1×10^5 cells/well) were seeded in 6-well plates for transfection.

Western blotting

Samples were lysed for total protein extraction in radioimmunoprecipitation buffer (Solarbio). The protein concentrations were detected by using a bicinchoninic acid protein assay kit (Thermo Fisher Scientific, Inc.). Equivalent amounts of protein (50 μg) were separated by SDS-PAGE and transferred onto polyvinylidene fluoride membranes (Merck KGaA). The membranes were incubated with primary antibodies, followed by a secondary antibody. Proteins were detected by using an enhanced chemiluminescence substrate kit (Thermo Scientific) and ImageJ software (NIH, Bethesda, MD). Detailed information of antibodies is shown in Supplementary Table S2.

Cell Counting Kit-8 and colony formation assays

Treated U251 or U87 cells (2×10^3 cells/well for Cell Counting Kit-8 (CCK-8) assays and 2×10^4 cells/well for colony formation assays) were seeded into 96- or 12-well plates and incubated in a 5% CO_2 atmosphere at 37°C. CCK-8 solution (Cat: HY-K0301-100T; MedChem Express, 15 μL/well) was added to each well at 0, 12, 24, 36, 48, 60, and 72 hours. After incubation for 3 hours, the optical density (OD) values were measured with a microplate reader (Bio-Tek) at 450 nm. Colony formation assays were conducted for 14 days, and the colonies were fixed in 70% ethanol for 10 minutes and then stained with 1% crystal violet solution for another 10 minutes at room temperature. Images were captured with a Nikon camera (Nikon 5300, Nikon Corporation).

Flow cytometer analysis

Treated U251 or U87 cells (2×10^5 cell/well) were seeded into 24-well plates and incubated overnight at 37°C. The cells were washed with PBS and resuspended in 0.5 mL binding buffer containing 5 μL annexin for 20 minutes in the dark for V-FITC and propidium iodide double staining (BD Biosciences). The apoptosis rate was measured with a FACSCalibur flow cytometer (BD Biosciences).

Wound-healing assay

Treated U251 or U87 cells (1.5×10^5 cells/well) were seeded into 6-well plates and cultured overnight at 37°C. A straight scratch was made by using a pipette tip. The cells were washed twice with PBS, and images were obtained as a baseline. Fresh medium was added, and images of the same location were acquired at 48 hours.

Transwell assay

Cell invasion abilities were detected by conducting Transwell assays. Transwell chambers were coated with Matrigel for 30 minutes at 37°C. Next, 200 μL treated cells were seeded into the upper chambers at a density of 2×10^3 cells/mL, and 700 μL complete medium was added to the lower chambers. After 48 hours, the noninvaded cells were removed. The cells on the lower side were washed three times with PBS, fixed in 4% paraformaldehyde for 30 minutes, and stained with crystal violet solution for 10 minutes. Images were captured under a microscope.

Luciferase reporter assay

Potential binding sites were predicted using the TargetScan database (http://www.targetscan.org). U87 cells (1×10^5 cells/well) were added to a 24-well plate and cotransfected with 200 ng pGL3-LUC-circNT5E or pGL3-LUC-control vector and 80 nmol miRNA mimics or miRNA-mutant mimics. After 48 hours of transfection, the cells were harvested, and luciferase activities were measured with the Dual-Luciferase Reporter Assay System (Promega).

Immunohistochemistry

All tissues were fixed overnight in a formalin solution, dehydrated in ethanol, embedded in paraffin, and sectioned at 5 μm. To remove the paraffin, the specimens were treated with xylene and ethanol. The slides were blocked with 5% normal goat serum and incubated with anti-ADARB2, anti-MMP-9, or anti-EGFR overnight at 4°C. After washing with PBS, the slides were incubated with goat anti-rabbit horseradish peroxidase (Vector Laboratories) for 30 minutes at room temperature. A DAB kit (Sigma-Aldrich) was used to detect the immunohistochemical (IHC) reactions. The slides were examined under a phase contrast light microscope (Nikon), and the average integral OD of each positively stained slide was measured using an Image-Pro plus 6.0 true color image analysis system. Three areas were chosen randomly from each section for measurement.

MRI detection

Briefly, samples were examined by enhanced MRI (3.0T, Siemens). The data were analyzed by using VBM, based on SPM5.

Animal studies

Four-week-old female BALB/c nude mice were purchased from the National Laboratory Animal Center. The animal studies were approved by the Institutional Animal Care and Use Committee of Pingjin Hospital. The mice were injected with U251 or U87 cells (2×10^6) that had been resuspended in growth media (150 μL) and Matrigel substrate (150 μL). The tumors were treated with lentiviral transduction 4 times at 9, 11, 13, and 16 hours after tumor formation. The animals were sacrificed at 37 days, and the tumors were collected to measure their weights and volumes. Tumor volume was measured and calculated with the formula: volume (mm^3) = length × width^2/2. All animals were maintained under specific pathogen-free conditions.

Statistical analysis

Data analyses were performed with SPSS software ver. 20.0 (SPSS, Inc.) and GraphPad Prism 7.0 (GraphPad Software. All experimental data are expressed as the mean ± SEM. Probability (P) values of <0.05 were considered statistically significant and were calculated using the Student t test as appropriate.

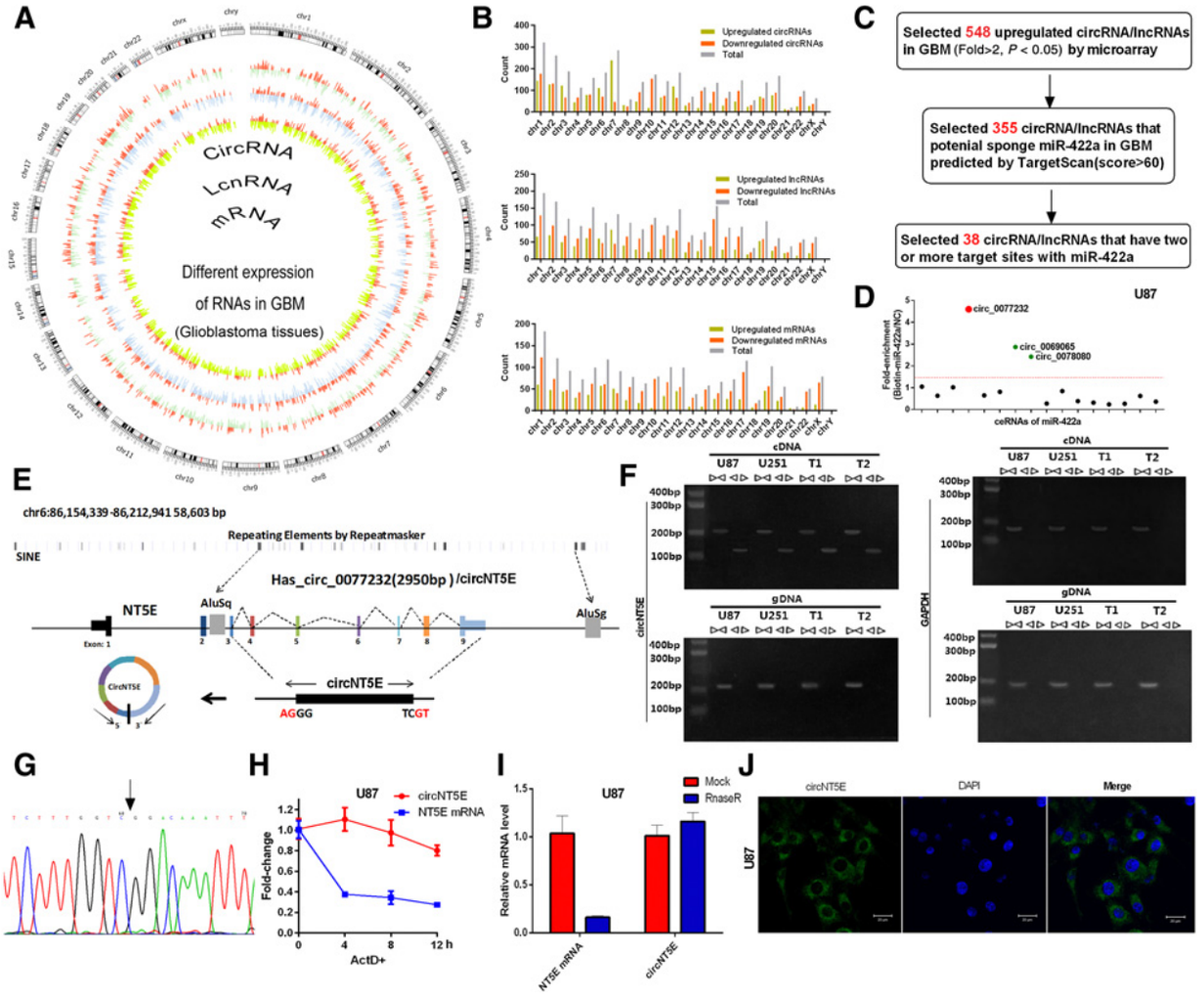

Figure 1.

circRNA, lncRNA, and mRNA profiling in human GBM tissues and circNT5E characterization. **A,** Differentially expressed RNAs (circRNAs, lncRNAs, and mRNAs) in GBM. **B,** Number of differentially expressed RNAs (circRNAs, lncRNAs, and mRNAs) in different chromosomes. Yellow-green bars, number of upregulated RNAs; saffron bars, number of downregulated RNAs; gray bars, number of total RNAs. **C,** Flowchart showing the steps used to screen circRNAs/lncRNAs that sponge miR-422a in GBM. **D,** Fold enrichment of 16 circRNAs/lncRNAs that were pulled down by biotin-miR-422a in U87 GBM cells. The three ceRNAs that were pulled down at 1.5-fold are indicated in green, and the most enriched ceRNA, circ_0077232, is indicated by red dots. **E,** Schematic diagram of the genomic location and splicing pattern of hsa_circ_0077232 (2,950 bp). **F,** The existence of circNT5E was validated in two GBM tumor tissue samples (T1 and T2) and U87 and U251 cell lines by RT-PCR. Divergent primers amplified circNT5E from cDNA, but not from genomic DNA (gDNA). GAPDH was used as a negative control. **G,** Arrow, "head-to-tail" splicing sites of circNT5E according to Sanger sequencing. **H,** circNT5E resistance to ActD was detected by qRT-PCR assay (ActD, actinomycin D). **I,** qRT-PCR was used to determine the abundance of circNT5E and linear NT5E mRNA in U87 cells treated with RNase R (normalized to mock treatment). **J,** RNA FISH showed the localization of circNT5E in U87 cells. DAPI solution was used to stain the nuclei; scale bars, 20 μm. The data in **H–I** are the mean ± SEM of three experiments.

Results

circRNA, lncRNA, and mRNA profiling in human GBM tissues and circNT5E characterization

First, we collected 3 pairs of clinical GBM samples (diagnosed by enhanced MRI) and isolated the total tissue RNA (Supplementary Fig. S1A and S1B). MiR-422a expression was confirmed to be lower in these 3 GBM tissue samples than in the matched normal brain tissues (Supplementary Fig. S1C). We further found that miR-422a was not regulated by promoter methylation and that 5′-azacytidine did not affect the expression level of miR-422a (Supplementary Fig. S1D). The three cases were subjected to microarray (circRNA, lncRNA, and mRNA) assays, and the Circos plots revealed differentially expressed circRNAs, lncRNAs, and mRNAs in GBM tissues compared with those in matched normal brain tissues (Fig. 1A). To validate these results, 6 circRNAs (hsa_circ_0001162, hsa_circ_0006774, hsa_circ_0077232, hsa_ circ_0006847, hsa_circ_0037751, and hsa_circ_0083682) and 6 lncRNAs (lnc-BET3L-2:1, NR_002734, NR_037144, NR_024442, NR_002791, and ENST00000398460) were selected randomly for qRT-PCR analysis. The results

indicated that the expression levels of the 6 lncRNAs and 6 circRNAs detected by qRT-PCR were consistent with those of the microarray assays (Supplementary Fig. S2). The results of the microarray detection were analyzed and classified. As shown in Supplementary Fig. S3A, the volcano plot indicated differentially expressed lncRNAs with significant differences (fold change > 2, $P < 0.05$, and a FDR < 0.05). A scatter plot also revealed differentially expressed lncRNAs in normal and tumor tissues (Supplementary Fig. S3B). The different lncRNAs were classified into six types according to the relationship and genomic loci with their associated coding genes (Supplementary Fig. S3C). The heatmap further reflected the differentially expressed lncRNAs in normal and tumor tissues (Supplementary Fig. S3D). The same analysis was performed for the different circRNAs, including volcano plot, scatter plot, and heatmap analyses (Supplementary Fig. S4A–S4C). A summary of the upregulated and downregulated circRNA, lncRNA, and mRNA in different chromosomes is shown (Fig. 1B). We selected the 548 upregulated circRNAs/lncRNAs in GBM (fold change > 2, $P < 0.05$, and a FDR < 0.05) by microarray for further analysis. The procedures used to screen the miR-422a–regulated ceRNAs are shown in Fig. 1C. Combined with the array data, we selected 355 circRNAs/lncRNAs that may function as sponges of miR-422a in GBM as predicted by TargetScan (score > 60). Thirty-eight circRNAs/lncRNAs were identified by analyzing the number of binding sites (two or more target sites with miR-422a). The Venn analysis results of these circRNAs/lncRNAs are shown in Supplementary Fig. S5A. Detailed information for the 38 circRNAs and lncRNAs associated with miR-422a is shown in Supplementary Fig. S5B. We experimentally tested these 38 circRNAs/lncRNAs in a GBM cell line by using the biotin-miRNA pull-down method (39). We designed 38 paired, specific primers (3 failed because they were highly homologous with the host gene and had a high GC content) to characterize the ceRNAs that could be pulled down by 3′-biotinylated miR-422a. The qRT-PCR results indicated 8 lncRNAs and 8 circRNAs with good specificity and repeatability. As shown in Fig. 1D, hsa_circ_0077232 showed high fold changes compared with the control group. Thus, we chose hsa_circ_0077232 for further analysis.

Hsa_circ_0077232 (circNT5E) is located in chromosome 6, is 2,950 base pairs (bp) in length, and consists of 7 exons (exons 3–9) from the NE5E genome (UCSC data in NCBI, Fig. 1E). To avoid trans-splicing or genomic rearrangements, including head-to-tail splicing, we used several universal circRNA detection methods (40). We first designed convergent primers to amplify NT5E mRNA and divergent primers to amplify circNT5E. Using cDNA and genomic DNA from two randomly selected GBM tissues and the U87 and U251 cell lines as templates, circNT5E was amplified from cDNA by only divergent primers (an expected 118-bp fragment), whereas no amplification product was observed from genomic DNA (Fig. 1F). Moreover, we confirmed the head-to-tail splicing in the RT-PCR product of circNT5E with the expected size by Sanger sequencing (Fig. 1G). To further confirm the circular characteristics of circNT5E, we added ActD, an inhibitor of transcription that degraded NT5E mRNA in U87 cells. As expected, circNT5E was more stable and resistant to ActD treatment (Fig. 1H). Furthermore, resistance to digestion with RNase R exonuclease confirmed that this RNA species is circular (Fig. 1I). FISH against circNT5E demonstrated that circNT5E preferentially localized in the cytoplasm (Fig. 1J).

CircNT5E affects the proliferation, apoptosis, migration, and invasion abilities of GBM

We detected circNT5E in normal, WHO I, WHO II, WHO III, and WHO IV glioma tissues by using FISH. The results showed that the expression level of circNT5E significantly increased as the clinical classification increased (Fig. 2A and B). qRT-PCR assays performed in paired GBM tumor tissues ($n = 18$) showed that circNT5E expression was significantly higher in tumor tissues than in normal tissues (Fig. 2C). These results indicate that circNT5E functions as an oncogene in glioma, thus prompting us to investigate the function of circNT5E. First, we examined the expression level of circNT5E in 4 GBM cell lines and found that circNT5E expression was the highest in U251 cells and lowest in U87 cells (Supplementary Fig. S6A). Thus, we chose the U87 and U251 cell lines for subsequent functional analyses. To explore the function of circNT5E in GBM cells, lentivirus-circNT5E (LV-circNT5E), LV-vector, LV-si-circNT5E, and LV-scrambled were constructed, and stable transfectants were established. qRT-PCR assays revealed that circNT5E was increased by 99.04-fold in U87-circNT5E–stable cell lines, whereas circNT5E was reduced by 77% in U251-si-circNT5E–stable cell lines compared with those in the control cells lines (Supplementary Fig. S6B and S6C). Cell viability, proliferation, apoptotic, invasion, and migration abilities were examined. The results indicated that the upregulation of circNT5E significantly promoted U87 cell growth, proliferation, invasion, and migration and inhibited apoptosis. While the knockdown of circNT5E significantly inhibited U251 cell growth, proliferation, invasion, and migration and promoted apoptosis (Fig. 2D–J; Supplementary Fig. S6D and S6E). These findings revealed that circNT5E promotes the growth, migration, and invasion of GBM cells *in vitro*.

CircNT5E promotes GBM tumor formation *in vivo*

We further investigated the effects of circNT5E on regulating tumor growth *in vivo*. A total of 2×10^6 U87 and U251 cells were subcutaneously injected into BALB/c nude mice (two groups, $n = 8$ each group). The procedure used for the animal study is shown in Fig. 3A. After injection, the mice were treated with LV-circNT5E or LV-si-circNT5E and their controls. Increased tumor sizes and weights were observed in the LV-circNT5E group compared with those in the LV-vector group (Fig. 3B–F). IHC staining showed that the expression of matrix metalloprotease (MMP)-9 and EGFR was increased by circNT5E (Fig. 3G–I). In addition, decreased tumor sizes and weights were observed in the LV-si-circNT5E group compared with those in the LV-scrambled group (Fig. 3J–N). MMP-9 and EGFR were inhibited by circNT5E knockdown (Fig. 3O–Q). Taken together, these results demonstrate that circNT5E efficiently promoted GBM tumor formation *in vivo*.

CircNT5E forms from the NT5E genome

The findings that circNT5E drives GBM cell tumorigenesis raise two important questions: which factors control its formation, and which factors (if any) regulate its overexpression in GBM? First, we investigated the mechanism by which circNT5E is formed. Ivanov and colleagues determined the circRNA biogenesis process and suggested that reverse complementary matches (RCM) are a conserved feature of circRNA biogenesis (41). According to a bioinformatic analysis of the 10-kb upstream/downstream sequence of circNT5E, we found that the flanking introns of NT5E

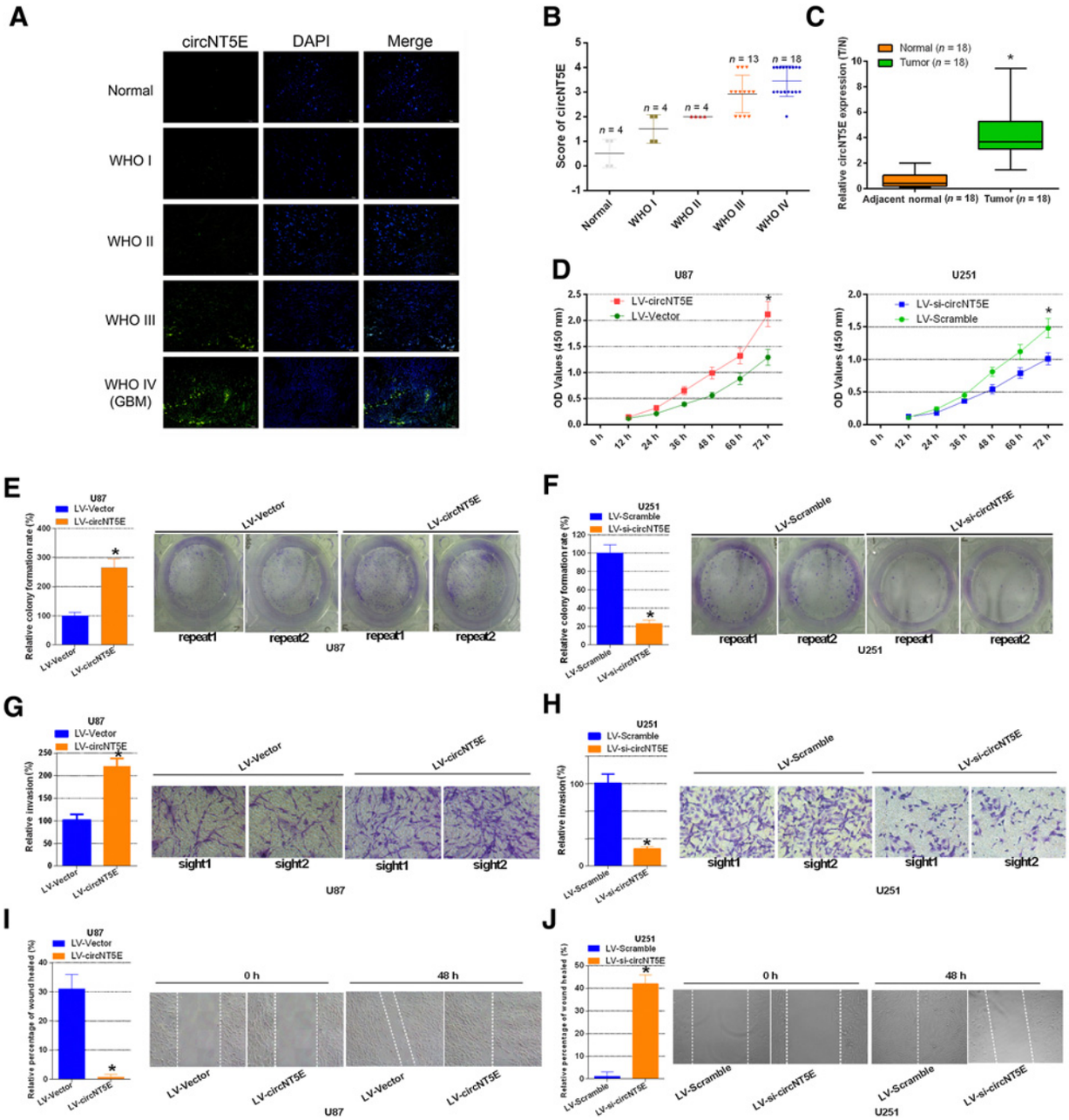

Figure 2.

CircNT5E affects the proliferation, apoptosis, migration, and invasion abilities of GBM. **A,** Representative FISH images showing circNT5E expression detected with a junction probe in normal, WHO I, WHO II, WHO III, and WHO IV GMB tissues; scale bars, 25 μm. **B,** FISH scores for circNT5E were determined for normal and WHO I–IV tissues. **C,** circNT5E expression was detected by qRT-PCR assay in 18 paired GBM tissues ($n = 18$; *, $P < 0.05$, paired Student t test). **D,** CCK-8 assays were used to determine cell viability in stable U87 cells transfected with LV-vector or LV-circNT5E and stable U251 cells transfected with LV-si-circNT5E or LV-scrambled. **E** and **F,** Cell proliferation ability was detected by colony formation assays in stable U87 and U251 cells; two representative images are shown. Colony formation rates were normalized to LV-vector or LV-scrambled group. **G** and **H,** Transwell assays were used to measure the invasion abilities of stable U87 and U251 cells; two representative images are shown (sight1 and sight2). **I** and **J,** Wound-healing assays were performed to detect the migration abilities of stable U87 and U251 cells. The data in **D–J** are the mean ± SEM of three experiments (*, $P < 0.05$, Student t test).

(exons 3–9) showed highly complementary Alu repeats with one short interspersed element (named Alusq) in the intron upstream of NT5E exon 3 and two short interspersed elements (named Alusg and AluJb) downstream of exon 9 (Supplementary Word S1). By using NCBI blast, the primate-specific Alusq and Alusg elements were found to be in an inverted orientation and highly reverse complementary (78% identity over 288 nucleotides (nt); Fig. 4A). Therefore, we hypothesized that the two reverse

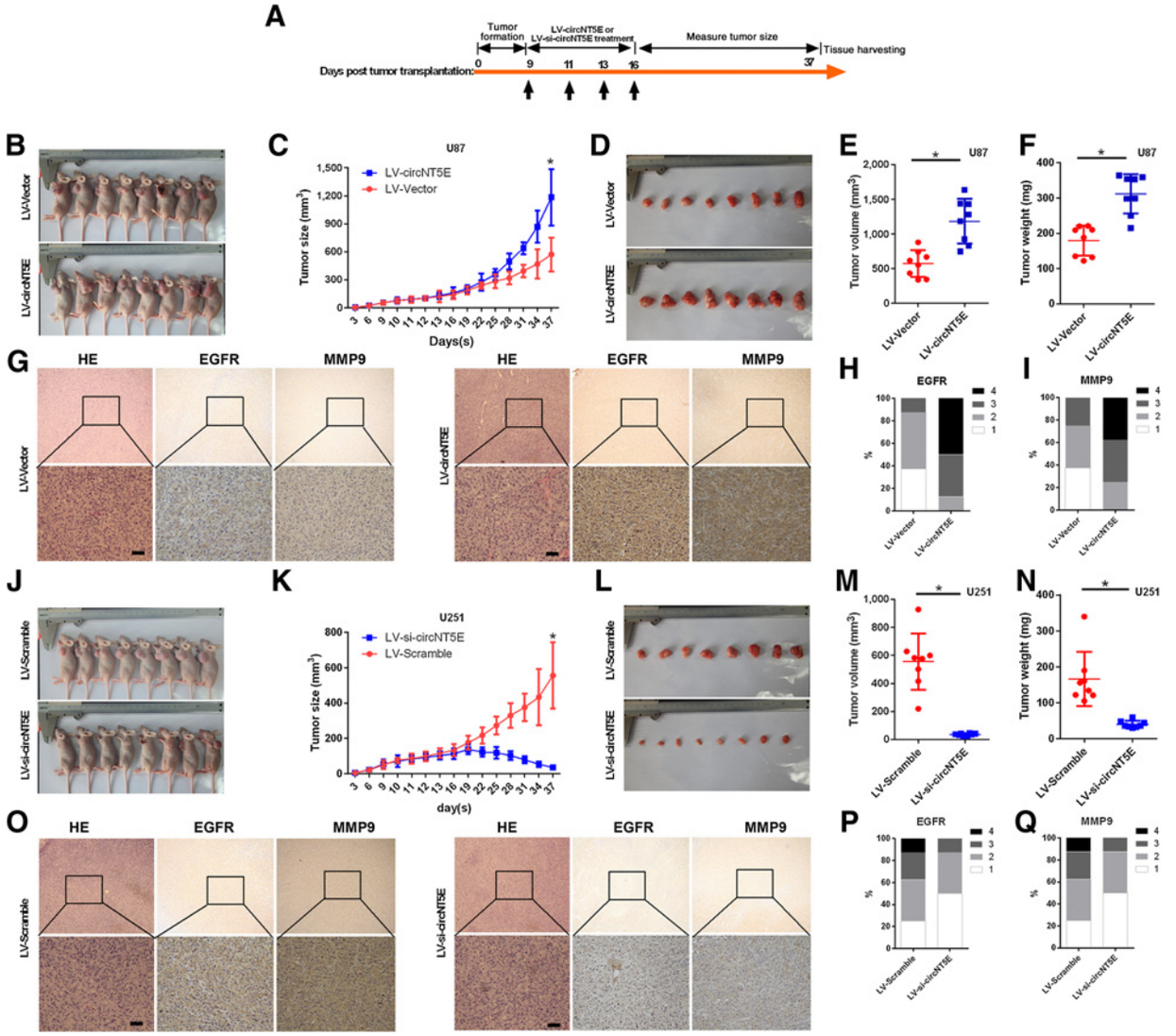

Figure 3.

CircNT5E promotes GBM tumor formation *in vivo*. **A,** Illustration of the LV-circNT5E and LV-si-circNT5E treatment timelines. The arrows indicate the four treatment times (9, 11, 13, and 16 days after transplantation). The divergent arrows indicate the different stages (first, tumor formation; second, lentiviral treatment; third, tumor size measurement). **B,** U87 cells (2×10^6 cells per mouse, $n = 8$ for each group) were inoculated in BALB/c nude mice to establish subcutaneous xenograft tumors. The mice were sacrificed at 37 days. **C,** The tumor sizes were also measured (*, $P < 0.05$). **D,** The dissected tumors were photographed. **E** and **F,** The tumor volumes and weights were measured at 37 days (*, $P < 0.05$). **G, H,** and **I,** IHC staining revealed that the overexpression of circNT5E led to increased EGFR and MMP-9 expression in the tumors; scale bars, 250 μm. **J–Q,** The same procedure was performed for U251 cells treated with LV-si-circNT5E and LV-scrambled. The data are the mean ± SEM of three experiments. *, $P < 0.05$ (Student *t* test).

complementary sequences mediate the circularization process of circNT5E, as suggested previously (42). Based on this hypothesis, we used CRISPR/Cas9 technology to delete some of the Alusq and Alusg sequence within GBM cells. First, we designed six guide RNAs (guide RNA 1, 2, and 3 and guide RNA 4, 5, and 6) to target Alusq and Alusg, respectively (Supplementary Fig. S7A). The efficiencies of the guide RNAs were determined by PCR analyses using primers flanking the targeted regions (F3/R3, F4/R4, F5/R5, F6/R6). Truncated genomic fragments were resolved by gel electrophoresis (Supplementary Fig. S7B). After validating the guide RNAs, we found that guide RNA1 (gRNA1) and gRNA2 removed 38 bases of the Alusq sequence, and gRNA4 and gRNA6 removed 101 bases of the Alusq sequence (Fig. 4B; Supplementary Fig. S7C and S7D). Furthermore, we screened stable Alusq/Alusg-truncated monoclonal U87 cells and then detected the formation of circNT5E. The results revealed that the expression level of circNT5E was decreased in gRNA1+2 (Clone2) and gRNA4+6 (Clone1) and nearly absent in gRNA1/2+4/6 (Clone4) compared with that in controls ($P < 0.05$, Fig. 4C–E). Moreover, we found that cell proliferation ability was significantly decreased in Alusq/Alusg-truncated monoclonal U87 cells compared with that in the control group (Fig. 4F–J). These results indicate that the long

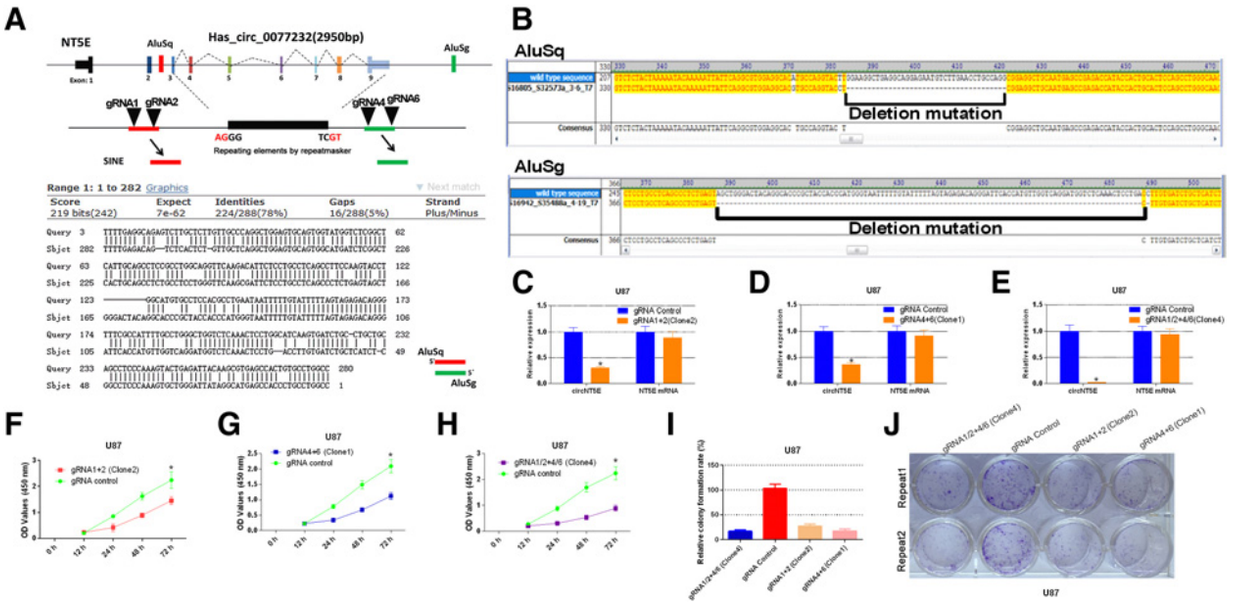

Figure 4.

CircNT5E is derived from NT5E exons 3–9 through long flanking introns. **A,** Top, the genomic regions of the NT5E exons 1–9 are shown with long introns flanking Alusq and Alusg. CRISPR/Cas9 systems (gRNA1 and 2 and gRNA 4 and 6) were designed to delete Alusq and Alusg, respectively. Bottom, NCBI BLAST results for Alusq and Alusg. **B,** The truncated sequences of the upstream Alusq and downstream Alusg were detected by Sanger sequencing. **C–E,** circNT5E and NT5E mRNA expression levels in stable U87 cells were detected by qRT-PCR assays. **F–H,** Proliferation in stable U87 cells was measured by using CCK-8 assays. **I** and **J,** Proliferation in stable U87 cells was measured by colony formation assays. The data in **C–J** are the mean ± SEM of three experiments (*, $P < 0.05$, Student *t* test).

flanking introns Alusq and Alusq are required for the formation of circNT5E.

CircNT5E is regulated by the RNA-editing enzyme ADARB2

We next examined which factors regulate the overexpression of circNT5E in GBM. Protein factors, such as Quaking, RNA-binding motif protein 20, and RNA-editing enzyme ADAR, that contribute to circRNA biogenesis have been identified in many previous studies (41, 43, 44). However, the factors that contribute to circRNA biogenesis in GBM progress are not well-understood. In the present study, we screened the original 3 paired GBM tissue mRNA chip results, as shown in the cluster heatmap (fold change >5 and $P < 0.01$ were used as strict screening criteria). We focused on the RNA-binding proteins and found that the specific brain-enriched RNA-editing enzyme ADARB2 was downregulated in GBM tissues (Fig. 5A). In the cohort of our clinical samples, we also found that ADARB2 mRNA was lower in GBM tissues than in normal brain tissues (Fig. 5B). However, unexpectedly, we found that the protein level of ADARB2 was higher in GBM tissues than in normal brain tissues by Western blot analysis (Fig. 5C). The IHC results also confirmed that the protein expression level of ADARB2 was higher in tumor tissues than in ANT (Fig. 5D). Next, we constructed an ADARB2 overexpression plasmid and transfected this plasmid into GBM cells to evaluate its effect on circNT5E. qRT-PCR and Western blot assays revealed the efficiency of the ADARB2 overexpression plasmid in U87 cells (Fig. 5E and F). The results showed that the expression levels of circNT5E were upregulated, whereas linear NT5E mRNA was downregulated in U87 cells with ADARB2 ectopic expression (Fig. 5G and H). These results suggest that ADARB2 is involved in the biogenesis of circNT5E in GBM.

Two important studies revealed that the RNA-editing enzyme ADAR1 is involved in circRNA biogenesis and that its knockdown may significantly upregulate circRNA expression in human HEK293 cells and SH-SY5Y cells (41, 45). First, we conducted RNAi targeting of ADAR1, which has been described in HEK293 and SH-SY5Y cells, to knock down ADAR1 in GBM cells. We found that circNT5E levels were increased by ADAR1 knockdown (Supplementary Fig. S8A), whereas ADAR1 overexpression decreased circNT5E levels (Supplementary Fig. S8B). These results are consistent with those of the previous study. However, we did not find ADAR1 dysregulation in the 3 paired GBM tissues of our microarray results. In addition, we found that ADARB2 could rescue ADAR1-induced circNT5E downregulation (Supplementary Fig. S8B). These results indicate that ADARB2 plays important roles and can rescue the ADAR1-induced circNT5E decrease in GBM cells. Furthermore, we performed RNA-binding protein immunoprecipitation (RIP) and RNA pull-down assays to evaluate whether ADARB2 binds to NT5E pre-mRNA. Following RIP, qRT-PCR demonstrated that ADARB2 binds directly to the long flanking introns of Alusq (Supplementary Fig. S8C). The RNA pull-down assay showed the same results (Supplementary Fig. S8D). Together, these data indicate that ADARB2 binds the pre-mRNA of NT5E and can rescue the ADAR1-induced downregulation of circNT5E.

CircNT5E functions as an efficient miR-422a sponge in GBM

Because circNT5E has been shown to play an important role in GBM tumorigenesis and is regulated by ADARB2, we next

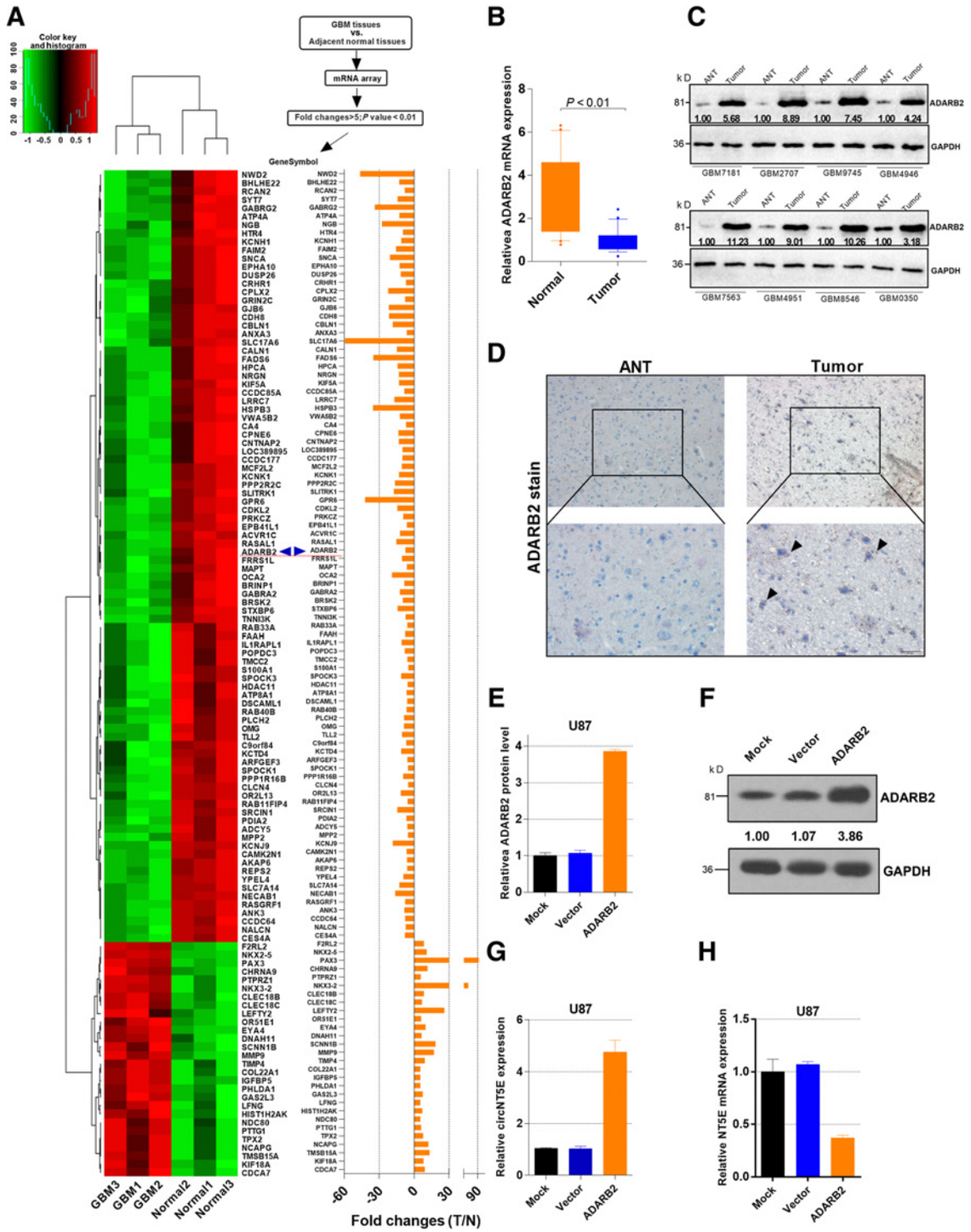

Figure 5.

CircNT5E is regulated by the RNA-editing enzyme ADARB2. **A,** Clustered heatmap of significantly differentially expressed mRNAs in GBM tissues and ANT (FC > 5, $P < 0.01$). Green, low expression; red, high expression. Arrows, RNA-binding protein ADARB2. **B,** ADARB2 mRNA expression was measured by qRT-PCR assays in GBM tumor tissues and normal tissues. **C** and **D,** The relative protein levels of ADARB2 were analyzed by Western blotting and immunohistochemistry in GBM tissues and ANT; representative images are shown. **E,** U87 cells were transfected with mock, pcDNA3, and ADARB2. The relative mRNA expression levels of ADARB2 were analyzed by qRT-PCR assays in treated U87 cells. **F,** The relative protein expression levels of ADARB2 were measured by Western blotting in treated U87 cells. **G** and **H,** The relative mRNA expression levels of circNT5E and linear NT5E mRNA were analyzed by qRT-PCR in treated U87 cells. The data are the mean ± SEM of three experiments (Student *t* test).

investigated the function of circNT5E in GBM cells. First, we determined that circNT5E could be pulled down by biotin-miR-422a in a ceRNA screening assay (Fig. 1D). Second, we searched circRNADB, a comprehensive database of human circular RNAs with protein-coding annotation, and found no results for circNT5E. Third, circNT5E is abundant and stable in the cytoplasm of GBM cells (Fig. 1J). Based on these findings, we predicted that circNT5E, which is 2,950 bp in length, serves as a binding platform for miRNAs, not just miR-422a. As predicted by TargetScan 6.2 and PubMed searches for "miRNA [AND] glioblastoma," we found 20 binding sites for miRNAs related to circNT5E (Fig. 6A). Nearly all miRNAs were GBM-related tumor suppressors that have been described previously (Supplementary Table S3). To identify the miRNAs that bind to circNT5E, we constructed a circNT5E expression vector containing a luciferase gene and transfected the vector into U87 cells. After transfection, we observed that 15 miRNAs, particularly miR-422a, showed downregulated expression (Fig. 6B). These results suggest that circNT5E functions as a sponge for GBM-related tumor-suppressor miRNAs. In addition, the pull-down assay suggested a 5.33-fold enrichment of circNT5E in the biotin-labeled miR-422a–captured fraction compared with that in the negative control, which is consistent with the results shown in Fig. 1D (Fig. 6C). Furthermore, the conventional luciferase reporter assay confirmed the interaction between circNT5E and miR-422a (Fig. 6D). qRT-PCR also confirmed that miR-422a expression was inversely related to circNT5E in stable LV-circNT5E U87 and LV-si-circNT5E U251 cells (Fig. 6E and F). A colocalization experiment further confirmed that circNT5E interacted with miR-422a (Fig. 6G). Moreover, two validated miR-422a targets, PIK3CA and NT5E, were found to be downregulated by the knockdown of circNT5E; the expression of these targets was rescued by cotransfection with miR-422a and circNT5E (Fig. 6H). Taken together, these results suggest that circNT5E binds directly to miR-422a and inhibits its activity.

CircNT5E affects the proliferation, apoptosis, invasion, and migration abilities of GBM cells via miR-422a

We further examined whether circNT5E functions as an oncogene by acting as a sponge of miR-422a. First, U87 cells were transfected with LV-vector+scrambled, LV-circNT5E+scrambled, LV-vector+miR-422a, and LV-circNT5E+miR-422a; U251 cells were transfected with LV-scrambled+anti-NC, LV-si-circNT5E+anti-NC, LV-scrambled+anti-422a, and LV-si-circNT5E+anti-422a. The transfection efficiency was determined by qRT-PCR (Fig. 7A and B). Subsequently, CCK-8, colony formation, apoptosis, and Transwell assays were performed. The results showed that miR-422a reversed the promoting effect of circNT5E on cell viability, proliferation, invasion, and migration and the inhibiting effect of circNT5E on cell apoptosis in GBM (Fig. 7C–J; Supplementary Fig. S9A and S9B). Based on these results, circNT5E affected the proliferation, apoptosis, invasion, and migration abilities of GBM cells, at least partly by miR-422a. Furthermore, we verified the effect of the circNT5E/miR-422a regulatory axis on its downstream signaling pathways by Western blot analysis. The results indicated that circNT5E upregulated the NT5E, SOX4, PI3KCA, p-Akt, and p-Smad2 levels in treated GBM cells, whereas circNT5E knockdown downregulated NT5E, SOX4, PI3KCA, p-Akt, and p-Smad2 levels (Fig. 7K). In addition, we also proved circNT5E regulated CDK4 and AURKA through miR-124 (Supplementary Fig. S10). Taken together, ADARB2 protein overexpression could reverse the ADAR1-induced circNT5E inhibition, which affected the survival, proliferation, migration, and invasion of GBM cells by regulating the miR-422a-NT5E, SOX4, and PI3KCA signaling pathways (Fig. 7L).

Discussion

Construction of the circRNA network in GBM

Previous studies from our group and other groups have shown that miR-422a is abnormally expressed in GBM and may act as a tumor suppressor in GBM (35, 38, 46). Unlike common screening microarrays in which tumor tissues and ANT are selected randomly, we selected 3 paired GBM tissues with low miR-422a expression and not regulated by methylation. Through the microarray analysis of RNAs in these specific GBM tissues, we detected thousands of circRNAs/lncRNAs that were dysregulated compared with those in their normal counterparts. These upregulated and downregulated circRNAs, lncRNAs, and mRNAs were in different chromosomes and formed the ceRNA network in GBM. We also validated the ceRNAs and detected many ceRNAs, including circNT5E, that were potential sponges of miR-422a in GBM. Combined with the results of a previous study showing that circRNAs are highly abundant and dynamically expressed in the mammalian brain (45), we found that specific circRNAs are candidate biomarkers and molecular targets for neurodegenerative diseases.

Identification and examination of the specific expression pattern of circNT5E

As ancient cyclic RNA molecules, circRNAs have been detected in RNA viruses as early as the 1970s (47, 48). However, the circRNA *CDR1as* was revealed in 2013 (13, 20). Currently, most circRNAs may originate from exons or introns (49) and are formed by exonic transcripts through gene rearrangement or nonlinear reverse splicing (50). These circRNAs cannot be degraded by the RNase R enzyme (51). These molecules have also been found to be tissue/developmental stage-specific and act as miRNA sponges that regulate gene expression (52). In our study, we identified a novel circRNA, termed circNT5E, in GBM pathology. We demonstrated that circNT5E was present in GBM tissues and cell lines and was resistant to ActD and RNase R. We found that circNT5E expression significantly increased as the clinical classification increased and that circNT5E significantly promoted the growth, proliferation, invasion, and migration and inhibited the apoptosis of GBM *in vivo* and *in vitro*. We also found that circNT5E requires RCMs for the circularization of NT5E by the CRISPR/CAS9 method. These results agree with those of previous studies (41). However, whether these RCMs matches are random or specific requires further investigation. In this study, we found that Alusq and Alusg were required for circNT5E formation, and this circularization promotes GBM tumorigenesis.

RNA-editing enzyme ADARB2 regulates circRNA expression

RCMs may structurally enable the formation of circNT5E, but the proteins regulating the specific expression of circNT5E are unknown. Only a few RCMs, such as muscleblind, QKI, and ADAR1, have been identified previously (41, 43, 45, 53). In our GBM cell lines, we found consistent results in which the knockdown of ADAR1 upregulated circNT5E (Supplementary Fig. S8A). However, the lack of ADAR1 dysregulation in our

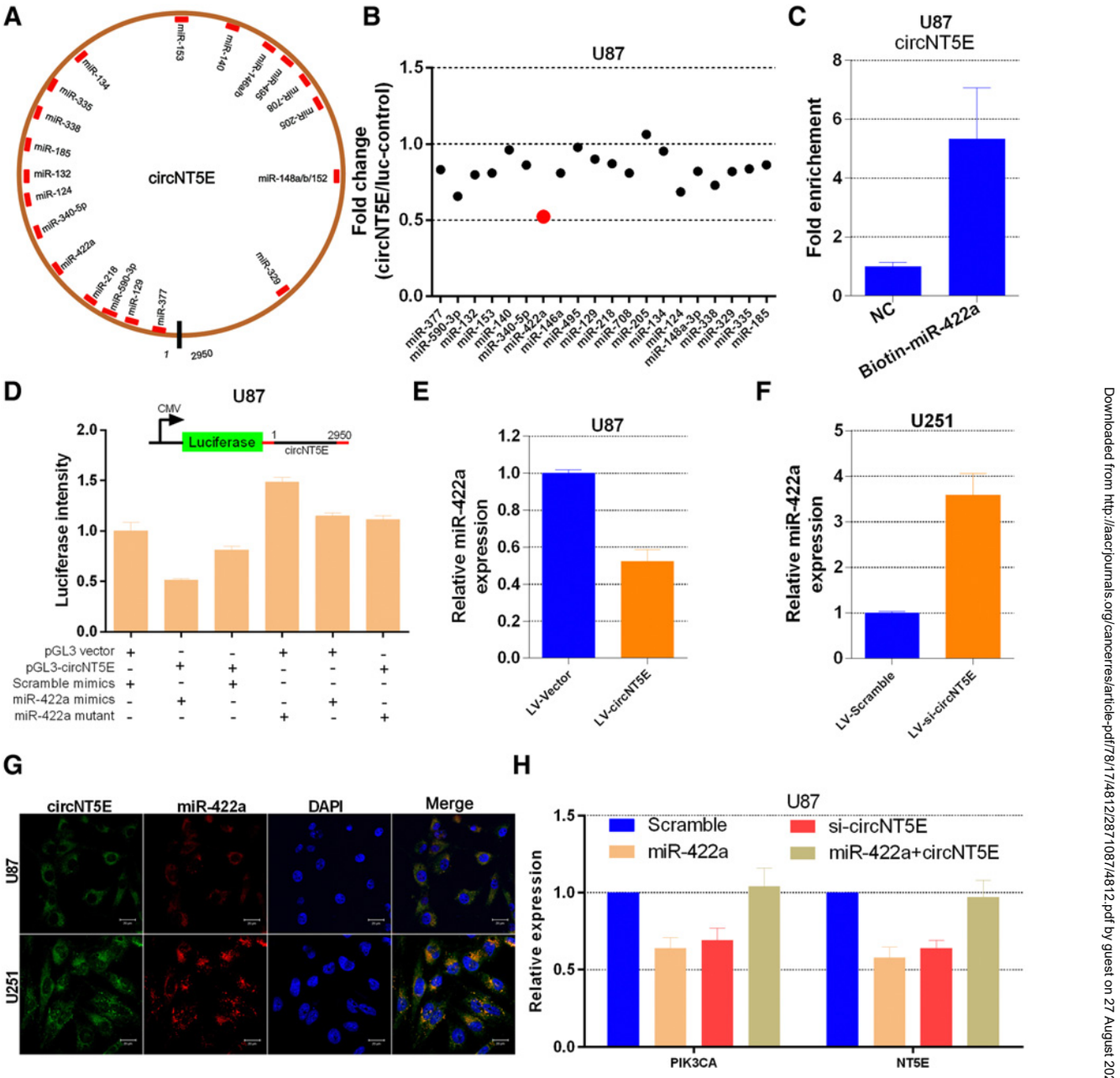

Figure 6.

CircNT5E functions as an efficient miR-422a sponge in GBM. **A,** Schematic drawing showing the putative binding sites of miRNAs related to circNT5E. **B,** U87 cells were cotransfected with LUC-circNT5E or LUC-vector (LUC-control). The expression of 20 miRNAs was detected by qRT-PCR. The fold change indicates miRNA expression in the LUC-circNT5E group/miRNA expression in the control group. The red dot indicates that miR-422a showed the greatest change following circNT5E treatment. **C,** qRT-PCR analysis of circNT5E levels in the streptavidin-captured fractions from U87 cell lysates after transfection with 3′-end biotinylated miR-422a or control (NC). **D,** U87 cells were cotransfected with pGL3 vector or pGL3-circNT5E and scrambled mimics, miR-422a mimics, or miR-422a mutant. Luciferase activity was detected with luciferase reporter assays. **E** and **F,** U87 cells were transfected with LV-vector and LV-circNT5E; U251 cells were transfected with LV-si-circNT5E and LV-scrambled. miR-422a expression levels were analyzed by qRT-PCR assays. **G,** Colocalization between miR-422a and circNT5E was observed by RNA *in situ* hybridization in U87 and U251 cells after cotransfection with circNT5E- and miR-422a–expressing vectors. The nuclei were stained with DAPI solution; scale bar, 20 μm. **H,** U87 cells were transfected with scrambled, miR-422a, si-circNT5E, or miR-422a+circNT5E. PIK3CA and NT5E mRNA expression levels were measured by qRT-PCR. The data in **C–H** are the mean ± SEM of three experiments (Student *t* test).

specific GBM tissues compared with the ANT (microarray data) could not explain the circNT5E upregulation; thus, further screening was conducted. Strict screening revealed ADARB2, a brain-specific member of the RNA-specific adenosine deaminase family (54). In our study, the microarray and qRT-PCR results showed that the ADARB2 transcript levels were lower in

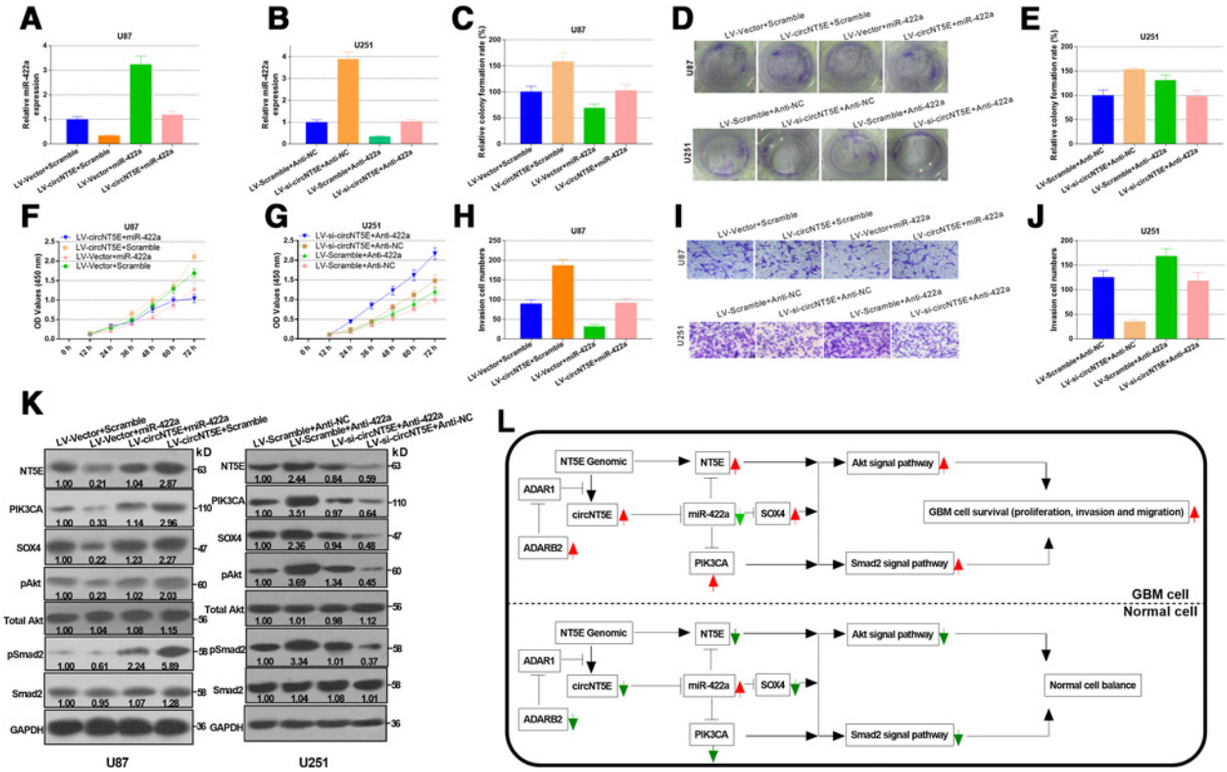

Figure 7.

CircNT5E regulates cell proliferation, migration, and invasion in GBM via miR-422a. **A** and **B,** U87 cells were transfected with LV-vector+scrambled, LV-circNT5E+scrambled, LV-vector+miR-422a, and LV-circNT5E+miR-422a; U251 cells were transfected with LV-scrambled+anti-NC, LV-si-circNT5E+anti-NC, LV-scrambled+anti-422a, and LV-si-circNT5E+anti-422a. miR-422a levels were examined by qRT-PCR. **C–E,** Proliferation in treated U87 and U251 cells was detected by colony formation assays. **F** and **G,** Proliferation in treated U87 and U251 cells was assessed by CCK-8 assays. **H–J,** Cell invasion in treated U87 and U251 cells was measured by Transwell invasion assays. **K,** Western blot assays were performed to measure the NT5E, PI3KCA, SOX4, p-Akt, total Akt, p-Smad2, and total Smad2 protein expression levels in treated U87 and U251 cells. GAPDH was used as an internal control. **L,** Schematic model of ADARB2-mediated circNT5E/miR-422a functions in GBM. The data in **A–J** are the mean ± SEM of three experiments (Student *t* test).

GBM tissues than in ANT, which is consistent with the results of a previous study (55, 56). However, unexpectedly, ADARB2 protein levels were higher in tumor tissues than in ANT according to the Western blotting and immunohistochemistry results, which is consistent with the results of a recent report (57). These results may be related to the complex regulatory mechanism of ADARB2 in GBM pathology. In this study, we clearly confirmed that ADARB2 binds to the NT5E pre-mRNA transcript and promotes the formation of circNT5E. These results support the recent hypothesis of Tan and colleagues (58) that suggests that ADARB2 is expressed in a brain-specific manner and has no enzymatic activity. Thus, ADARB2 may act as a suppressor of ADAR family members.

Support for the ceRNA hypothesis in GBM

Studies of circRNA/lncRNA functions in human disease through the ceRNA mechanism have generated substantial interest, not only as a potential global mechanism but also as a mechanism explaining the function of any RNA. However, the entire transcriptome of human disease is required to study ceRNA. Herein, we identified circNT5E by the transcriptome screening of circRNAs, lncRNAs, and mRNAs; circNT5E may serve as a modulator of GBM tumorigenesis by sponging multiple miRNAs (Fig. 6A and B; Supplementary Fig. S10), particularly miR-422a. Our results indicated that one circRNA may be associated with a variety of miRNAs. Thus, large amounts of circRNAs may provide a platform for harboring miRNAs, such as circNT5E and circHIPK3 (26). These results also support that ceRNAs contain few miRNA-binding sites (<5) for natural miRNAs, which is a common phenomenon in mammals (59). However, this ceRNA mechanism remains controversial (27), and additional studies of circRNAs as ceRNAs in human diseases are needed.

Conclusion

The major findings of this study are as follows: (1) We determined the circRNA/lncRNA expression profiles in GBM tumorigenesis. (2) Screening revealed a sponge of miR-422a, circNT5E, that regulates GBM cell proliferation, invasion, and migration. (3) We characterized and functionally evaluated whether circNT5E is formed from the NT5E genome and regulated by the RNA-editing enzyme ADARB2. (4) Our findings suggest that circNT5E exerts additional regulatory functions by sponging GBM suppressor miRNAs. Taken together, these results provide insights into developing novel treatment approaches for GBM.

Data availability

The microarray data have been deposited in Gene Expression Omnibus database under accession code GSE109569. All other data that support the findings of this study are available from the corresponding authors upon reasonable request.

Disclosure of Potential Conflicts of Interest

No potential conflicts of interest were disclosed.

Authors' Contributions

Conception and design: R. Wang, H. Liang
Development of methodology: R. Wang, X. Chen, J. Li, R. Jia, H. Liang
Acquisition of data (provided animals, acquired and managed patients, provided facilities, etc.): R. Wang, X. Chen, R. Jia, Y. Pan, H. Liang
Analysis and interpretation of data (e.g., statistical analysis, biostatistics, computational analysis): R. Wang, N. Li, J. Li, Y. Pan, H. Liang
Writing, review, and/or revision of the manuscript: R. Wang
Administrative, technical, or material support (i.e., reporting or organizing data, constructing databases): R. Wang, S. Zhang, X. Chen, N. Li, J. Li, R. Jia, H. Liang
Study supervision: R. Wang, S. Zhang, X. Chen, H. Liang

Acknowledgments

We thank the ceRNA microarray support of Shanghai Biotechnology Cooperation. We thank the lentivirus and plasmids support of Genepharma Biotechnology Co., Ltd. We thank the nude mice platform support of Tianjin Saier Co., Ltd. We thank the kindly support of the CRISPR/Cas9 plasmids from Professor Zhao Qingshun (Nanjing University).

This work was supported by the National Natural Science Foundation of China (No. 81502183 to R. Wang); Key projects of Tianjin Municipal Commission of Health and Family Planning (No. 16KG137 to H. Liang); and Project of the Affiliated Hospital of Logistics University of Chinese People's Armed Police Force (FYZ201602 to H. Liang, FYM201602 to R. Wang).

The costs of publication of this article were defrayed in part by the payment of page charges. This article must therefore be hereby marked *advertisement* in accordance with 18 U.S.C. Section 1734 solely to indicate this fact.

Received February 19, 2018; revised April 24, 2018; accepted June 19, 2018; published first July 2, 2018.

References

1. Malzkorn B, Reifenberger G. Practical implications of integrated glioma classification according to the World Health Organization classification of tumors of the central nervous system 2016. Curr Opin Oncol 2016; 28:494–501.
2. Louis DN, Perry A, Reifenberger G, von Deimling A, Figarella-Branger D, Cavenee WK, et al. The 2016 World Health Organization classification of tumors of the central nervous system: a summary. Acta Neuropathol 2016; 131:803–20.
3. Stupp R, Mason WP, van den Bent MJ, Weller M, Fisher B, Taphoorn MJ, et al. Radiotherapy plus concomitant and adjuvant temozolomide for glioblastoma. N Engl J Med 2005;352:987–96.
4. Weller M, van den Bent M, Hopkins K, Tonn JC, Stupp R, Falini A, et al. EANO guideline for the diagnosis and treatment of anaplastic gliomas and glioblastoma. Lancet Oncol 2014;15:e395–403.
5. Prust ML, Jafari-Khouzani K, Kalpathy-Cramer J, Polaskova P, Batchelor TT, Gerstner ER, et al. Standard chemoradiation in combination with VEGF targeted therapy for glioblastoma results in progressive gray and white matter volume loss. Neuro-oncol 2018;20:289–91.
6. Weller M, Butowski N, Tran DD, Recht LD, Lim M, Hirte H, et al. Rindopepimut with temozolomide for patients with newly diagnosed, EGFRvIII-expressing glioblastoma (ACT IV): a randomised, double-blind, international phase 3 trial. Lancet Oncol 2017;18: 1373–85.
7. Guttman M, Rinn JL. Modular regulatory principles of large non-coding RNAs. Nature 2012;482:339–46.
8. Batista PJ, Chang HY. Long noncoding RNAs: cellular address codes in development and disease. Cell 2013;152:1298–307.
9. Sabin LR, Delás MJ, Hannon GJ. Dogma derailed: the many influences of RNA on the genome. Mol Cell 2013;49:783–94.
10. Ulitsky I, Bartel DP. lincRNAs: genomics, evolution, and mechanisms. Cell 2013;154:26–46.
11. Anastasiadou E, Jacob LS, Slack FJ. Non-coding RNA networks in cancer. Nat Rev Cancer 2018;18:5–18.
12. Zhang XO, Dong R, Zhang Y, Zhang JL, Luo Z, Zhang J, et al. Diverse alternative back-splicing and alternative splicing landscape of circular RNAs. Genome Res 2016;26:1277–87.
13. Memczak S, Jens M, Elefsinioti A, Torti F, Krueger J, Rybak A, et al. Circular RNAs are a large class of animal RNAs with regulatory potency. Nature 2013;495:333–8.
14. Zhu LP, He YJ, Hou JC, Chen X, Zhou SY, Yang SJ, et al. The role of circRNAs in cancers. Biosci Rep 2017;37.
15. Pamudurti NR, Bartok O, Jens M, Ashwal-Fluss R, Stottmeister C, Ruhe L, et al. Translation of CircRNAs. Mol Cell 2017;66:9–21 e7.
16. Hanan M, Soreq H, Kadener S. CircRNAs in the brain. RNA Biol 2017;14:1028–34.
17. Granados-Riveron JT, Aquino-Jarquin G. The complexity of the translation ability of circRNAs. Biochim Biophys Acta 2016;1859: 1245–51.
18. Lasda E, Parker R. Circular RNAs: diversity of form and function. RNA (New York, NY) 2014;20:1829–42.
19. Qu S, Yang X, Li X, Wang J, Gao Y, Shang R, et al. Circular RNA: a new star of noncoding RNAs. Cancer Lett 2015;365:141–8.
20. Hansen TB, Jensen TI, Clausen BH, Bramsen JB, Finsen B, Damgaard CK, et al. Natural RNA circles function as efficient microRNA sponges. Nature 2013;495:384–8.
21. Du WW, Yang W, Liu E, Yang Z, Dhaliwal P, Yang BB. Foxo3 circular RNA retards cell cycle progression via forming ternary complexes with p21 and CDK2. Nucleic Acids Res 2016;44:2846–58.
22. Legnini I, Di Timoteo G, Rossi F, Morlando M, Briganti F, Sthandier O, et al. Circ-ZNF609 is a circular RNA that can be translated and functions in myogenesis. Mol Cell 2017;66:22–37 e9.
23. Yang Y, Gao X, Zhang M, Yan S, Sun C, Xiao F, et al. Novel role of FBXW7 circular RNA in repressing glioma tumorigenesis. J Natl Cancer Inst 2018;110.
24. Zhang M, Huang N, Yang X, Luo J, Yan S, Xiao F, et al. A novel protein encoded by the circular form of the SHPRH gene suppresses glioma tumorigenesis. Oncogene 2018;37:1805–14.
25. Wang K, Long B, Liu F, Wang JX, Liu CY, Zhao B, et al. A circular RNA protects the heart from pathological hypertrophy and heart failure by targeting miR-223. Eur Heart J 2016;37:2602–11.
26. Zheng Q, Bao C, Guo W, Li S, Chen J, Chen B, et al. Circular RNA profiling reveals an abundant circHIPK3 that regulates cell growth by sponging multiple miRNAs. Nat Commun 2016;7:11215.
27. Thomson DW, Dinger ME. Endogenous microRNA sponges: evidence and controversy. Nat Rev Genet 2016;17:272–83.
28. Hsiao KY, Lin YC, Gupta SK, Chang N, Yen L, Sun HS, et al. Noncoding Effects of Circular RNA CCDC66 promote colon cancer growth and metastasis. Cancer Res 2017;77:2339–50.
29. Han D, Li J, Wang H, Su X, Hou J, Gu Y, et al. Circular RNA circMTO1 acts as the sponge of microRNA-9 to suppress hepatocellular carcinoma progression. Hepatology 2017;66:1151–64.
30. Zheng J, Liu X, Xue Y, Gong W, Ma J, Xi Z, et al. TTBK2 circular RNA promotes glioma malignancy by regulating miR-217/HNF1beta/Derlin-1 pathway. J Hematol Oncol 2017;10:52.
31. Yu J, Xu QG, Wang ZG, Yang Y, Zhang L, Ma JZ, et al. Circular RNA cSMARCA5 inhibits growth and metastasis in hepatocellular carcinoma. J Hepatol 2018;68:1214–27.
32. Yang P, Qiu Z, Jiang Y, Dong L, Yang W, Gu C, et al. Silencing of cZNF292 circular RNA suppresses human glioma tube formation via the Wnt/beta-catenin signaling pathway. Oncotarget 2016;7:63449–55.

33. Lewis BP, Burge CB, Bartel DP. Conserved seed pairing, often flanked by adenosines, indicates that thousands of human genes are microRNA targets. Cell 2005;120:15–20.
34. Salmena L, Poliseno L, Tay Y, Kats L, Pandolfi PP. A ceRNA hypothesis: the rosetta stone of a hidden RNA language? Cell 2011;146:353–8.
35. Liang H, Wang R, Jin Y, Li J, Zhang S. MiR-422a acts as a tumor suppressor in glioblastoma by targeting PIK3CA. Am J Cancer Res 2016;6:1695–707.
36. Bonnin N, Armandy E, Carras J, Ferrandon S, Battiston-Montagne P, Aubry M, et al. MiR-422a promotes loco-regional recurrence by targeting NT5E/CD73 in head and neck squamous cell carcinoma. Oncotarget 2016;7:44023–38.
37. Molina-Pinelo S, Gutierrez G, Pastor MD, Hergueta M, Moreno-Bueno G, Garcia-Carbonero R, et al. MicroRNA-dependent regulation of transcription in non-small cell lung cancer. PLoS One 2014;9:e90524.
38. Wang H, Tang C, Na M, Ma W, Jiang Z, Gu Y, et al. miR-422a inhibits glioma proliferation and invasion by targeting IGF1 and IGF1R. Oncol Res 2017;25:187–94.
39. Lal A, Thomas MP, Altschuler G, Navarro F, O'Day E, Li XL, et al. Capture of microRNA-bound mRNAs identifies the tumor suppressor miR-34a as a regulator of growth factor signaling. PLoS Genet 2011;7:e1002363.
40. Jeck WR, Sharpless NE. Detecting and characterizing circular RNAs. Nat Biotechnol 2014;32:453–61.
41. Ivanov A, Memczak S, Wyler E, Torti F, Porath HT, Orejuela MR, et al. Analysis of intron sequences reveals hallmarks of circular RNA biogenesis in animals. Cell reports 2015;10:170–7.
42. Liang D, Wilusz JE. Short intronic repeat sequences facilitate circular RNA production. Gen Develop 2014;28:2233–47.
43. Conn SJ, Pillman KA, Toubia J, Conn VM, Salmanidis M, Phillips CA, et al. The RNA binding protein quaking regulates formation of circRNAs. Cell 2015;160:1125–34.
44. Khan MA, Reckman YJ, Aufiero S, van den Hoogenhof MM, van der Made I, Beqqali A, et al. RBM20 regulates circular RNA production from the titin gene. Circ Res 2016;119:996–1003.
45. Rybak-Wolf A, Stottmeister C, Glazar P, Jens M, Pino N, Giusti S, et al. Circular RNAs in the mammalian brain are highly abundant, conserved, and dynamically expressed. Mol Cell 2015;58:870–85.
46. Li R, Gao K, Luo H, Wang X, Shi Y, Dong Q, et al. Identification of intrinsic subtype-specific prognostic microRNAs in primary glioblastoma. J Exp Clin Cancer Res 2014;33:9.
47. Wu Q, Wang Y, Cao M, Pantaleo V, Burgyan J, Li W-X, et al. Homology-independent discovery of replicating pathogenic circular RNAs by deep sequencing and a new computational algorithm. Proc Natl Acad Sci 2012;109:3938–43.
48. Wilusz JE, Sharp PA. A circuitous route to noncoding RNA. Science (New York, NY) 2013;340:440.
49. Zhang Y, Zhang X-O, Chen T, Xiang J-F, Yin Q-F, Xing Y-H, et al. Circular intronic long noncoding RNAs. Mol Cell 2013;51:792–806.
50. Salzman J, Gawad C, Wang PL, Lacayo N, Brown PO. Circular RNAs are the predominant transcript isoform from hundreds of human genes in diverse cell types. PLoS One 2012;7:e30733.
51. Salzman J, Chen RE, Olsen MN, Wang PL, Brown PO. Cell-type specific features of circular RNA expression. PLoS Genet 2013;9:e1003777.
52. Militello G, Weirick T, John D, Doring C, Dimmeler S, Uchida S. Screening and validation of lncRNAs and circRNAs as miRNA sponges. Brief Bioinform 2017;18:780–8.
53. Ashwal-Fluss R, Meyer M, Pamudurti NR, Ivanov A, Bartok O, Hanan M, et al. circRNA biogenesis competes with pre-mRNA splicing. Mol Cell 2014;56:55–66.
54. Melcher T, Maas S, Herb A, Sprengel R, Higuchi M, Seeburg PH. RED2, a brain-specific member of the RNA-specific adenosine deaminase family. J Biol Chem 1996;271:31795–8.
55. Paz N, Levanon EY, Amariglio N, Heimberger AB, Ram Z, Constantini S, et al. Altered adenosine-to-inosine RNA editing in human cancer. Genome Res 2007;17:1586–95.
56. Roversi G, Pfundt R, Moroni RF, Magnani I, van Reijmersdal S, Pollo B, et al. Identification of novel genomic markers related to progression to glioblastoma through genomic profiling of 25 primary glioma cell lines. Oncogene 2006;25:1571–83.
57. Oakes E, Anderson A, Cohen-Gadol A, Hundley HA. Adenosine deaminase that acts on RNA 3 (ADAR3) binding to glutamate receptor subunit B Pre-mRNA Inhibits RNA editing in glioblastoma. J Biol Chem 2017;292:4326–35.
58. Tan MH, Li Q, Shanmugam R, Piskol R, Kohler J, Young AN, et al. Dynamic landscape and regulation of RNA editing in mammals. Nature 2017;550:249–54.
59. Tay Y, Rinn J, Pandolfi PP. The multilayered complexity of ceRNA crosstalk and competition. Nature 2014;505:344–52.